Int. J. Multiphase Flow Vol. 13, No. 6, pp. 773–784, 1987
Printed in Great Britain.

0301-9322/87 $3.00 + 0.00

LATERAL MIGRATION MECHANISMS IN CAPILLARY HYDRODYNAMIC CHROMATOGRAPHY

H. J. PLOEHN
Department of Chemical Engineering, Princeton University, Princeton, NJ 08544, U.S.A.

(*Received* 11 *November* 1986; *in revised form* 27 *June* 1987)

Abstract—In all chromatographic systems that achieve separation of colloidal particles based on the particles' hydrodynamic behavior, there are partitioning mechanisms that promote lateral migration of particles across solvent streamlines. In this work, solvent inertia and particle electrostatics are incorporated in Brenner & Gaydos' general diffusive transport theory for particles and solvent flowing in a capillary, yielding the mean axial velocity of particles as a function of particle size. A comparison is made with capillary hydrodynamic chromatography results. The lateral migration of small particles is primarily due to diffusion, while large particles are focused by the inertial force at one equilibrium radial position, as observed in "tubular pinch" experiments. The transition from diffusion- to inertia-controlled lateral migration can be tuned to specific particle size ranges through variation of solvent ionic strength, flowrate and capillary radius. Poor prediction of the separation behavior of large particles is attributed to inaccuracy in the calculation of the inertial radial velocity, suggesting the need for further theoretical analysis and experimental study of inertial migration.

INTRODUCTION

The flow of suspensions of particles, drops or bubbles through narrow ducts is of central importance in many areas of science and technology. One application is the characterization of the size, chemistry and polydispersity of colloidal particles through the use of chromatography. Given the diversity of colloidal phenomena, a variety of chromatographic techniques have been developed; these are reviewed by McHugh (1984). The focus of this work will be on those techniques that utilize the particles' hydrodynamic behavior, known generically as hydrodynamic chromatography (HDC).

DiMarzio & Guttman (1969, 1970) originally suggested that chromatographic separation could be achieved solely due to particle hydrodynamics. This proposal was brought to fruition in the experimental work of Small (1974), who coined the term "hydrodynamic chromatography". Subsequent theoretical work modeled Small's packed-bed chromatographic column as a bundle of parallel capillary tubes. Such models naturally suggest the use of a single, narrow capillary tube as the chromatographic column. This technique, called "capillary hydrodynamic chromatography" (CHDC), was implemented by several groups (Mullins & Orr 1978; Brough *et al.* 1981; Noel *et al.* 1982; Tijssen *et al.* 1983). However, no complete theoretical analysis of CHDC, including particle diffusion, fluid inertia and electrostatic force, has yet appeared in the literature.

The separation mechanism of CHDC can be rationalized in terms of the lateral migration of particles across the capillary. As a particle is convected down the capillary by the solvent flow, it is also subject to Brownian motion, causing the particle to sample radial positions and streamlines. Due to the particle's finite size, it cannot sample the streamlines closest to the wall and consequently moves at a rate faster than the average solvent velocity. Larger particles sample fewer slow streamlines and are eluted before smaller particles. Brenner & Gaydos (1977) show that particles sample radial positions not at random but with a probability given by a Boltzmann distribution which depends upon the external forces acting on the particles. The Brenner–Gaydos theory provides the foundation for the analysis of packed-bed HDC as realized in the work of Stoisits *et al.* (1976), Silebi & McHugh (1978), Prieve & Hoysan (1978) and Nagy *et al.* (1981).

Noel *et al.* (1982) and McHugh (1984) have speculated as to the nature of lateral migration mechanisms active in CHDC. Differences in the elution characteristics of particles with radii $\gtrsim 1\ \mu m$ lead to the hypothesis that the lateral migration of small particles is diffusion controlled, while the migration of large particles is controlled by fluid inertia. Inertial effects are

the cause of the "tubular pinch effect" first reported by Segré & Silberberg (1962a, b). Saffman (1956), Brenner & Happel (1958) and Bretherton (1962) have shown that there can be no lateral migration of large (non-diffusing) particles across undisturbed solvent streamlines if solvent inertia is neglected. Early theoretical analyses of inertial migration, reviewed by Leal (1980), concentrate on particle lateral migration in Couette or parallel-plate geometries. Cox & Brenner (1968) present a solution of the Navier–Stokes equation for a single particle carried by flow in a duct; specialization to a spherical particle in Poiseuille flow in a cylinder has been reported by Ishii & Hasimoto (1980).

Utilizing the inertial radial velocity results of Ishii & Hasimoto (1980) as well as the particle–cylinder wall-effect tensors developed by Hirschfeld *et al.* (1984), this work incorporates fluid inertial effects and particle–capillary electrostatic interactions within the framework of the Brenner–Gaydos (1977) diffusive transport theory, yielding a better understanding of the lateral migration mechanisms in CHDC.

ANALYSIS

The goal of the Brenner & Gaydos (1977) theory is the modification of the Taylor–Aris theory of axial dispersion (Taylor 1953, 1954; Aris 1956) to include the effects of particle hydrodynamics and external forces on the mean axial velocity and dispersivity of the solute. The principal result of interest here is the expression for the mean particle axial velocity:

$$\langle u_z \rangle = \frac{\int_0^{R_0 - a} u_z(r)\, e^{-E(r)} r\, dr}{\int_0^{R_0 - a} e^{-E(r)} r\, dr}, \qquad [1]$$

where R_0 is the capillary radius, a is the particle radius, u_z is the local axial velocity of the particle and E is the dimensionless total potential experienced by the particle due to interactions with the capillary wall. There interactions may be divided into two categories: colloidal and hydrodynamic. The former, including electrostatic and van der Waals forces, are conservative forces that can be integrated to give potentials for use in [1]. Hydrodynamic forces, especially in systems dominated by viscous effects, are dissipative; it is not clear *a priori* whether such interactions are within the purview of the Brenner–Gaydos analysis. The work of Cox & Brenner (1968) and Ishii & Hasimoto (1980) shows that solvent inertia produces a lateral (i.e. radial) particle velocity that depends on radial position. Division by the particle's radial mobility gives an inertial force, and integration yields an inertial "potential" which, of course, is not a true potential. Nonetheless, a simple modification of the Brenner–Gaydos analysis demonstrates that the inertial "potential" may be included in the total potential of [1].

The original Brenner–Gaydos analysis assumes that the particle velocity has only an axial component. Instead, let the particle velocity be given by the vector sum

$$\mathbf{u}(r) = \mathbf{e}_r u_r(r) + \mathbf{e}_z u_z(r) \qquad [2]$$

of the radial and axial velocity components u_r and u_z. The new radial velocity term is carried through the Brenner–Gaydos development, finally appearing in the equation for the axisymmetric probability density $f(r, z, t)$; f is the probability density that a particle is located within dr and dz of position (r, z) while within dt of time t. The equation for f is not actually solved; rather, Aris' (1956) method of moments is used to calculate $\langle u_z \rangle$.

Defining the mth axial moment of $f(r, z, t)$ through

$$\mu_0(r, t) = \int_{-\infty}^{\infty} z^m f(r, z, t)\, dz \qquad [3]$$

the steady-state zeroth-order moment is found to be

$$\mu_0(r) = \frac{c}{2\pi} \exp\left\{ -\left[E_n - \frac{1}{kT} \int \frac{u_r(r')}{M_\perp(r')}\, dr' \right] \right\}, \qquad [4]$$

in which $c/2\pi$ is a normalization constant, E_n is the non-inertial part of the total potential and $M_\perp$

is the hydrodynamic mobility of particles perpendicular to the cylinder axis. The radial velocity, representing the hydrodynamic response of the particle to the inertial force exerted by the fluid, has been calculated for the sphere–cylinder geometry by Ishii & Hasimoto (1980), based on a general theory by Cox & Brenner (1968). The function $M_\perp$, as utilized by Brenner & Gaydos (1977), is related to the Stokes flow wall-effect tensor of Hirschfeld *et al.* (1984) through

$$M_\perp(r) = \frac{1 - \left(\frac{a}{R_0}\right) W_{11}(r)}{6\pi\mu a}, \qquad [5]$$

in which $\mathbb{W}$ is the tabulated wall-effect tensor and μ is the solvent viscosity. Hirschfeld *et al.* (1984) relate the radial force to the radial velocity through

$$F_i(r) = \frac{u_r(r)}{M_\perp(r)}, \qquad [6]$$

in which the subscript i is a reminder that, in this case, the force is due to inertia via the radial velocity. The inertial "potential" is defined through

$$E_i(r) = -\frac{1}{kT}\int_{r^*}^{r} F_i(r')\,dr', \qquad [7]$$

where r^* is the dimensionless radial position where the inertial force is zero; combining [4], [6] and [7] produces

$$\mu_0(r) = \frac{c}{2\pi}\exp\left[-\left(E_e + E_i\right)\right] = \frac{c}{2\pi}\exp(-E), \qquad [8]$$

as was found by Brenner & Gaydos (1977). Equation [1] then follows without any change from the original Brenner–Gaydos analysis.

Calculation of the mean particle axial velocity requires specification of the local particle axial velocity, $u_z(r)$, any non-inertial potential that may be important and the inertial potential due to the fluid motion in the sphere–cylinder geometry. The local axial velocity of a particle in a cylinder is

$$u_z(r) = 2v_m\left(1 - \frac{r^2}{R_0^2}\right) - \gamma v_m \lambda^2, \qquad [9]$$

where v_m is the average solvent axial velocity, $\lambda = a/R_0$ and γ is the wall-effect parameter, given by

$$\gamma = \frac{4}{3}\left(1 + \frac{3r}{R_0}\right) \qquad \text{(core region)} \qquad [10a]$$

$$= \frac{5}{4}\frac{\lambda}{\left(1 - \frac{r}{R_0}\right)^2} \qquad \text{(wall region)} \qquad [10b]$$

$$= \frac{2}{\lambda^2}\left[1 - \frac{0.7431}{0.6376 - 0.2\ln\left(\frac{1}{\lambda} - \frac{r}{a} - 1\right)}\right] + \left(1 - \frac{r^2}{R_0^2}\right) \qquad \text{(very close to the wall)}, \qquad [10c]$$

as developed by Brenner (1966) and Goldman *et al.* (1967).

If the ionic strength of the (aqueous) solvent phase is low, electrostatic repulsion is the dominant contribution to the non-inertial part of the potential. When $\lambda \ll 1$, the interaction between the spherical particle and the surrounding capillary can be approximated by a sphere–plane interaction. The dimensionless electrostatic potential in this case, for a symmetric 1–1 electrolyte, is given by Bell *et al.* (1970) as

$$E_e(r) = \frac{4\pi\epsilon_r\epsilon_0 kT}{e^2} a Y_1 Y_2 \exp[-\kappa(R_0 - a - r)], \qquad [11a]$$

$$Y_i = 4\tanh\left(\frac{\Psi_i}{4}\right), \qquad [11b]$$

$$Y_2 = Y_2(\Psi_2, a\kappa), \tag{11c}$$

$$\Psi_i = \frac{e\psi_i}{kT}, \tag{11d}$$

in which ϵ_r is the relative permittivity of the solvent, ϵ_0 is the permittivity of vacuum, e is the electronic charge, $1/\kappa$ is the Debye double-layer thickness, and ψ_1 and ψ_2 are the electrostatic surface potentials for the capillary and the particle. The Debye length, $1/\kappa$, may be found from

$$\kappa^2 = \frac{2e^2n}{\epsilon_r\epsilon_0 kT}, \tag{12}$$

where n is the number density of ionic species in a 1–1 symmetric electrolyte. Ohshima *et al.* (1982) have derived an approximate surface charge density–surface potential relationship,

$$\sigma_s = 2\left(\frac{\epsilon_r\epsilon_0\kappa kT}{e}\right)\left\{1 + \frac{2}{a\kappa\cosh^2\left(\frac{\Psi_i}{4}\right)} + \frac{8\ln\left[\cosh\left(\frac{\Psi_i}{4}\right)\right]}{a^2\kappa^2\sinh^2\left(\frac{\Psi_i}{2}\right)}\right\}^{\frac{1}{2}}\sinh\left(\frac{\Psi_i}{2}\right), \tag{13}$$

valid for spherical particles. If the surface charge density, σ_s, is regarded as the controlling parameter, then [13] can be solved for Ψ_i. The particle function Y_2 depends on the surface potential through

$$Y_2 = 8\tanh\left(\frac{\Psi_2}{4}\right)\left\{1 + \left[1 - \frac{2a\kappa + 1}{(1+a\kappa)^2}\tanh^2\left(\frac{\Psi_2}{4}\right)\right]^{\frac{1}{2}}\right\}^{-1}, \tag{14}$$

also given by Ohsima *et al.* (1982). Y_1 is calculated from [11b] if the capillary and particle surface potentials are assumed to be the same.

The inertial potential, E_i, found from [5]–[7], depends on the radial velocity, u_r, the radial mobility, $M_\perp$, and the equilibrium radial position, r^*. The radial velocity of neutrally buoyant particles involves complicated integrals that were evaluated numerically by Ishii & Hasimoto (1980); $u_r(r)$ is presented graphically, with r^* found from the zero point of u_r. Rather than duplicating these calculations, we utilize Ishii & Hasimoto's approximate expression

$$u_r(r) = \alpha\lambda^2\left(\frac{av_m^2\rho}{\mu}\right)\frac{r}{R_0}\left(r^* - \frac{r}{R_0}\right) \tag{15}$$

in which selection of $\alpha = 3.56$ and $r^* = 0.71$ produce an accurate fit of their numerical results (see their figure 4a). Here ρ is the solvent density. The predicted value of r^* is independent of particle size since their analysis is only valid for asymptotically small particles; $r^* = 0.71$, as is shown below, leads to the prediction that large particles pass through the capillary more slowly than the solvent, on average. On the other hand, the tubular pinch results summarized by Walz & Grun (1973) indicate that r^* varies with solvent flowrate and particle size for neutrally buoyant particles, and that the particles are eluted faster than an average unit of solvent. In lieu of rigorous calculation of u_r and r^* for larger particle sizes, we must employ some empiricism in order to obtain at least qualitative agreement with experiment. The empirical relation

$$r^* = 0.67(1 - \lambda)q(v_m) \tag{16}$$

is proposed by Walz & Grun (1973) to correlate most of the equilibrium radial position data from tubular pinch experiments. The flowrate function $q(v_m)$ is given by an exponential function adjusted to fit Ishii & Hasimoto's (1980) theoretical variation of r^* with v_m, shown in their figure 6a.

For particle positions near the capillary wall, the radial velocity of Cox & Hsu (1977),

$$u_r(r) = -\frac{5}{72}\frac{av_m^2\rho}{\mu}\mu^2\beta^2(1-\beta)(22 - 73\beta), \tag{17}$$

with $\beta = 1 - r/R_0$, is used in place of [15].

Equation [15] provides a convenient characteristic radial velocity $\tilde{u}_r = \lambda^2(av_m^2\rho/\mu)$. Defining the dimensionless quantities

$$\xi \equiv \frac{r}{R_0}, \quad U \equiv \frac{u_r}{\tilde{u}_r}, \quad m_\perp \equiv 6\pi\mu a M_\perp, \tag{18}$$

[5]–[7] and [18] are combined to produce

$$E_i(\xi) = -\text{Pé} \int_{r^*}^{\xi} \frac{U(\xi')}{m_\perp(\xi')} d\xi', \quad [19]$$

where the Péclet number

$$\text{Pé} = \frac{6\pi\rho v_m^2 a^3 \lambda^2}{kT} \quad [20]$$

represents the ratio of inertial to diffusive forces acting on the particle.

RESULTS AND DISCUSSION

Calibration curves, the standard means of presenting particle separation data from CHDC experiments, give the particle radius as a function of the retention ratio, which equals $v_m/\langle u_z \rangle$. Values of the retention ratio < 1 imply that the particles pass through the capillary faster, on average, than the solvent.

A comparison of experimental and theoretical calibration curves is shown in figure 1. The points are the experimental values of Noel *et al.* (1982) for a variety of particles (primarily pollens and polystyrene latices) carried by water with 1% ethylene glycol added as a surfactant. The solid curves are calculated from [1] using the local particle axial velocity, electrostatic potential and inertial potential described earlier. Evaluation of the Péclet number via [20] indicates that Pé $\approx O(1)$ for 1 μm radius particles. The dependence of Pé on a^3 suggests that as particle size increases, there is a rapid transition from diffusion-controlled to inertia-controlled lateral migration, supporting the hypothesis of Noel *et al.* (1982) and McHugh (1984). Also, Noel *et al.* observed that there is a minimum solvent flowrate below which particle size resolution is poor, presumably due to insufficient separation forces. This behaviour is explained by the v_m^2 dependence of Pé which produces a diffusion–inertia transition with increasing solvent velocity.

Curve A of figure 1 is a theoretical calibration curve found using [16] for r^*. Agreement for small particles is good, but for large particles, the experimental retention ratios are poorly predicted by the calculated values. This failure is certainly due to error in the calculation of the inertial radial velocity. The restrictions of the Cox–Brenner/Ishii–Hasimoto analysis must be carefully examined.

Assuming that all of the particles in the experiments of Noel *et al.* (1982) have the same density as polystyrene, the solvent flowrates are such that Brenner's (1972) neutral buoyancy criterion

$$\frac{U_{sed}}{v_m} \ll \lambda^2 \quad [21]$$

is satisfied for all particle sizes, although the sedimentation velocity

$$U_{sed} = \frac{2a^2(\rho_p - \rho)g}{9\mu} \quad [22]$$

(with ρ_p as the particle density) is non-zero. The Cox–Brenner/Ishii–Hasimoto analysis requires

$$\text{Re}_p \ll \lambda \ll 1 \quad [23]$$

with the particle Reynolds number

$$\text{Re}_p = \frac{a u_s \rho}{\mu} \quad [24]$$

based on the relative velocity u_s (the difference between the local undisturbed solvent velocity and the local particle axial velocity). The condition $\lambda \ll 1$ is easily satisfied in Noel *et al.*'s experiments, but, utilizing the greatest anticipated relative velocity, the condition $\text{Re}_p \ll \lambda$ is violated for large particles near the capillary wall. Consequently, there is a region in the flow where fluid inertia is as important as viscosity (the Oseen region). Thus the Ishii–Hasimoto inertial radial velocity is not strictly correct for large particles, and [15] and [16] are expected to fail at some point as particle size increases and fluid inertia becomes more than a perturbation in the creeping flow calculations.

For large particles, the Péclet number [20] indicates that inertial migration is the dominant lateral

migration mechanism; as is illustrated below, large particles are essentially "locked in" at the radial position r^* and are eluted at the same speed as solvent at that radial position. The form of the radial velocity, such as that of [15], becomes less relevant than the value of r^*. Since there is no accurate expression for u_r when $Re_p \simeq \lambda$, one might try to fit the calibration curve for large particles by retaining the form of [15] and modifying that of [16]. If an *ad hoc* parameter δ is introduced, so that

$$r^* = 0.67(1 - \lambda^\delta)q(v_m), \qquad [25]$$

selection of $\delta = 0.65$ yields the calibration curve B of figure 1. This fit is probably not unique, but the exercise suggests the probability of a more complicated dependence of r^* on λ than has been previously found, either theoretically or experimentally.

Another assumption in the use of the Brenner–Gaydos equation [1] is that the particle hydrodynamic behavior reaches a steady state. In terms of the Stokes particle diffusivity, $D_\infty = kT/6\pi\mu a$, the criterion for steady-state behavior is

$$\frac{D_\infty t}{R_0^2} \gg 1, \qquad [26]$$

suggesting that particles must be in the capillary long enough to sample all radial positions. Reformulating this criterion in terms of the length of capillary necessary to assure steady-state behavior gives

$$L_{req} = \frac{6\pi\mu a R_0^2 v_m}{kT}. \qquad [27]$$

McHugh (1984) observes that L_{req} is at least 2 orders of magnitude greater than the capillary length used by Noel *et al.* (1982). This criterion, though, is appropriate when diffusion is dominant. We define a characteristic inertial time

$$t_i = \frac{R_0}{\lambda^2 \frac{v_m^2 a\rho}{\mu}}, \qquad [28]$$

where the denominator is the characteristic inertial radial velocity from [18]. The capillary length that assures steady-state behavior with respect to inertia,

$$L_{req} = \frac{\mu}{\lambda^3 \rho v_m}, \qquad [29]$$

is comparable to or less than the capillary lengths used by Noel *et al.* Although transient lateral migration certainly influences the theoretical retention ratio, the effect is probably not large enough to account for the difference between the experimental retention ratios for large particles and those of curve A in figure 1.

Particle–particle interactions at finite concentrations also influence the lateral migration of particles, but no quantitative studies of the effect in CHDC are available. The particle concentrations in the CHDC experiments of Noel *et al.* (1982) are unknown, but we presume that the experiments were not carried out at infinite dilution where the present analysis applies. Speculation on the consequences of concentration effects should be based on consideration of colloidal and hydrodynamic forces. In Noel *et al.*'s experiments, the use of ethylene glycol as a surfactant reduces particle aggregation and adsorption on the capillary wall; low ionic strength (I) also opposes aggregation, but the actual electrostatic conditions are not known. Particle hydrodynamic interactions may be most significant. As described in detail by Happel & Brenner (1983), an assemblage of particles has a lower resistance to flow than a single particle. Thus two or more interacting particles will have a lower relative velocity than a singlet, leading to a lower retention ratio. Since Brownian motion randomizes the positions of small particles, the decrease in retention ratio due to concentration effects is probably greater for large particles controlled by inertia.

The general shape of the theoretical calibration curves can be rationalized by considering the individual contribution of each lateral migration mechanism. This comparison is shown in figure 2. Curve A is the calibration curve for particles that are perfectly free to diffuse to any radial

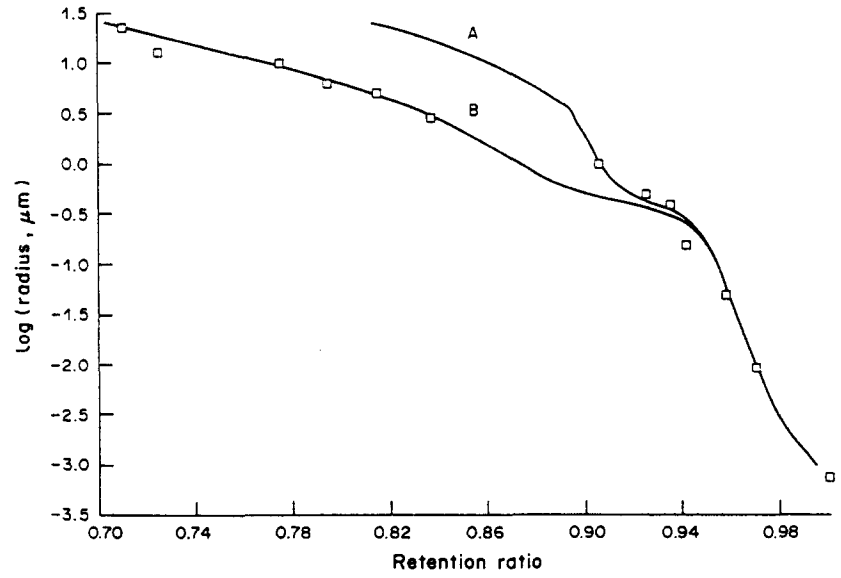

Figure 1. Calibration curves for the CHDC system studied by Noel *et al.* (1982). The points are the experimental data of Noel *et al.* for various pollens and polystyrene lattices carried by water with 1% ethylene glycol added as a surfactant. The solid curves are the calculated calibration curves from the present model. Curve A: r^* calculated from [16]. Curve B: r^* calculated from [25]. Relevant parameters include: $R_0 = 254\ \mu m$, $v_m = 0.1713$ m/s, $I = 2 \times 10^{-7}$ M, $\sigma_s = 10^{13}$ charges/cm^2, $\rho_p = 1.05$ g/cm^3, $T = 20$°C.

position that their finite size permits; i.e. curve A shows only the effect of volume exclusion. As expected, the larger the particle, the faster it passes through the capillary relative to the solvent. The calibration curve of particles free to diffuse under the influence of the electrostatic potential is curve B. Electrostatic repulsion causes particles of all sizes to be further excluded from regions of slow solvent flow, speeding up the particles' passage through the capillary. Curve C is the calibration curve for diffusing particles under the influence of only the inertial potential. Large particles are essentially "locked in" at the equilibrium radial position and translate at the local particle axial velocity evaluated at r^*, i.e. $\langle u_z \rangle = u_z(r^*)$. This explanation is supported by the

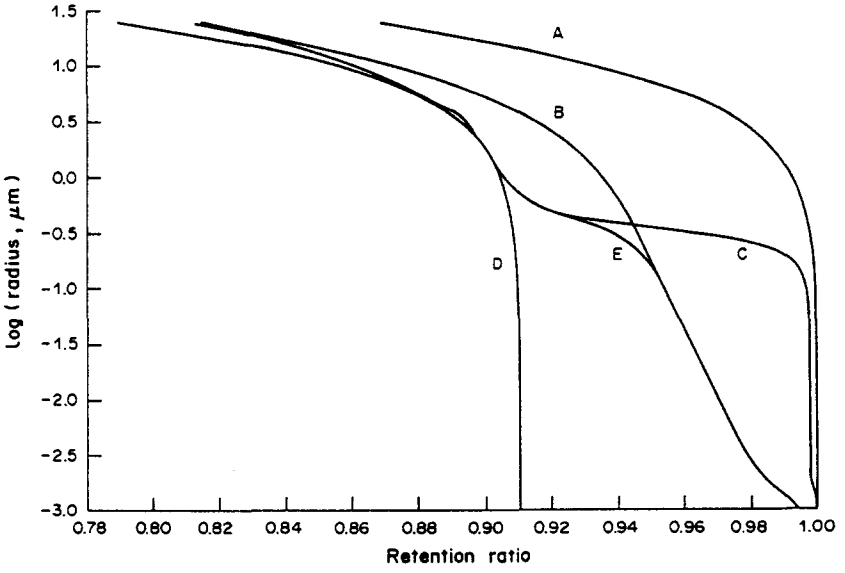

Figure 2. Calibration curves highlighting the individual contributions of diffusion, electrostatics and fluid inertia to particle lateral migration. Curve A: diffusion with volume exclusion effect only. Curve B: diffusion under the influence of an electrostatic potential. Curve C: diffusion under the influence of an inertial potential. Curve D: particles translate at the solvent velocity evaluated at r^*. Curve E: total curve including the contributions of all mechanisms. All parameters are the same as in figure 1.

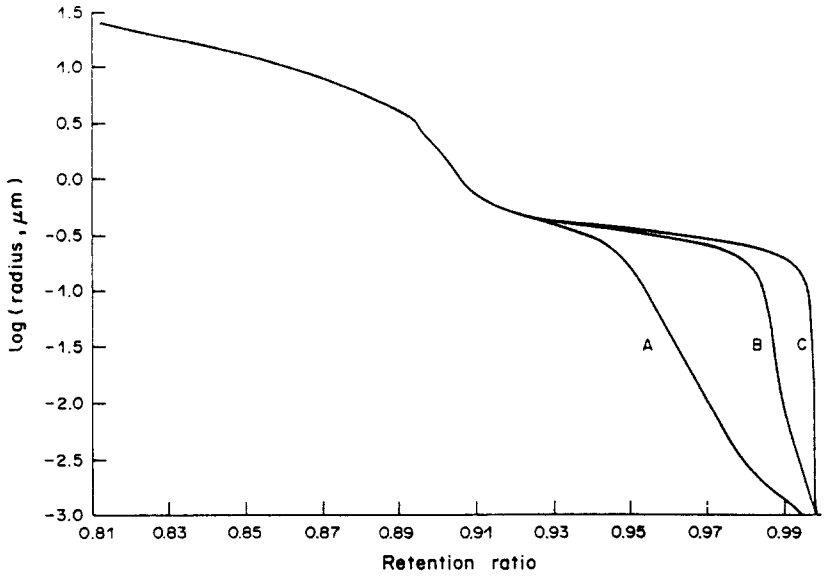

Figure 3. Calibration curves for three solvent ionic strengths, all other parameters the same as in figure 1. Curves A–C are for $I = 10^{-7}$, 10^{-6} and 10^{-5} M, respectively.

calculation of curve D, the calibration curve of particles that travel at the *solvent* velocity evaluated at the equilibrium radial position. For small particles, [16] indicates that $r^* \rightarrow 0.67$ (neglecting the flowrate dependence for the moment). A simple calculation utilizing the Poiseuillian solvent velocity profile shows that $v_m/u_z\,(0.67) = 0.91$, the limiting value of the retention ratio of curve D. For large particles, curves C and D are almost the same: the slight difference in retention ratio is due to the significant axial relative velocity of large particles. Returning to curve C, the Brownian motion of particles with radii $< \sim 1\ \mu$m causes the particles to diffuse out of the inertial potential well into slower flow regions. The smallest particles, although somewhat affected by inertia, separate primarily due to the volume exclusion effect. The total curve including all effects is curve E.

The variation of the theoretical calibration curve with respect to changes in several of the system parameters are shown in the next three figures. Figure 3 illustrates the effect of solvent ionic strength on particle separation. As expected, an increase in the ionic strength decreases the range and strength of the electrostatic repulsion; the smallest particles can then penetrate close to the wall and are separated due to the volume exclusion effect. Note that as ionic strength is increased, the retention ratio range in which both inertia and diffusion are important is expanded. The resolution of the elution peaks (i.e. the separability) of submicron particles can therefore be improved through the use of moderate ionic strength solvents. However, ionic strength has little effect on the elution of large particles, consistent with the conclusions of Brough *et al.* (1981).

The effect of variation of the capillary radius at constant ionic strength is illustrated in figure 4. As the capillary radius is made smaller, λ increases and, through [16], r^* decreases. Particles focused at r^* due to the inertial potential are shifted towards the capillary centerline and move faster relative to the solvent. An interesting effect is observed in narrow capillaries with low solvent ionic strengths (curve A in figure 4): the calibration curve is no longer monotonic. In general, as the particle radius decreases, the particles begin to diffuse out of the inertial potential well located at r^*. Particles diffuse into both faster and slower streamlines, but the slower streamlines are weighted more heavily due to the factor r in the integrals of [1]. This explains the general increase of retention ratio with decreasing particle size found in most calibration curves. For the separation described by curve A in figure 4, however, the retention ratio increases only until the particle radius falls to about 0.3 μm. For smaller particles, increased Brownian motion causes particles to sample the faster streamlines, but the electrostatic potential excludes particles from the slower streamlines. The retention ratio therefore begins to increase with decreasing particle size. This behavior is only noticeable in smaller capillaries in which the electrostatic repulsion dominates a larger fraction of

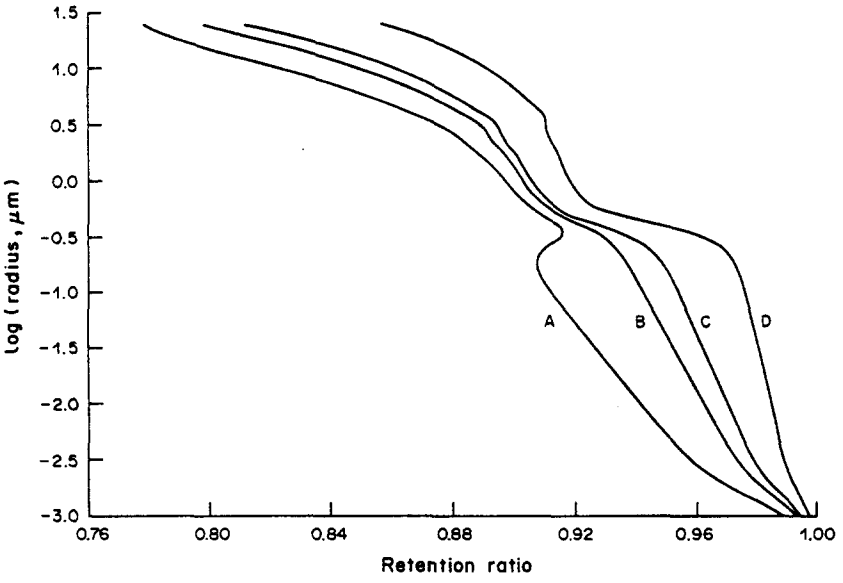

Figure 4. Calibration curves for four capillary radii (i.d.), all other parameters the same as in figure 1. Curves A–D are for $R_0 = 125$, 200, 250 and 500 μm, respectively.

the streamlines. As diffusion becomes more important ($a \approx 0.2\,\mu$m, Pé ≈ 0.1) all of the fast streamlines are sampled, and smaller particles begin to penetrate further into the slow region of flow. The usual separation behavior for small particles is then observed.

Finally, the effect of changes in the solvent flowrate on the calibration curve is shown in figure 5. For small particles the inertial force is weak and flowrate has little effect on the separation characteristics. The separation of large particles depends weakly on flowrate, through the value of r^* given by [16]. The effect of flowrate variation is most pronounced for particle sizes in the transition region between inertially- and diffusion-controlled separation. This transition occurs at Pé $\approx O(1)$; since Pé depends on the square of the mean solvent velocity, the flowrate has a strong influence on the location of the transition. At constant particle radius there appears to be critical flowrate above which particles are inertially focused at the equilibrium radial position, consistent with experimental observations. For 1 μm particles, the flowrates of curves A and B produce

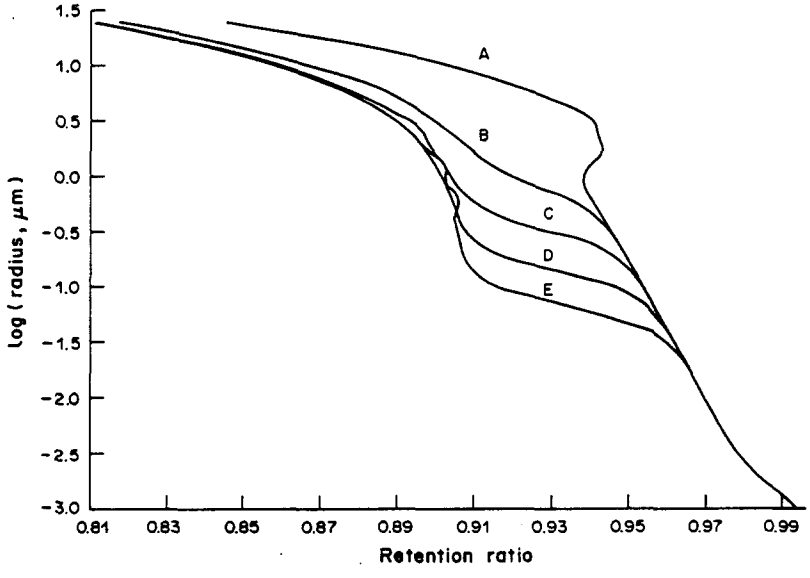

Figure 5. Calibration curves for five solvent flowrates, all other parameters the same as in figure 1. Curves A–E are for $v_m = 0.01$, 0.05, 0.25, 1.25 and 5.00 m/s, respectively.

insufficient inertial force to focus the particles at r^*. Also, as noted earlier, the flat portion of the calibration curve is an indication of enhanced separability. Adjustment of the flowrate, solvent ionic strength or capillary radius can be used to vary the location of the transition region, improving separability in specific particle size ranges.

CONCLUSION

The results presented here have important implications with regard to the use of CHDC as an analytical tool. First, electrostatic forces play a larger role in capillary particle separations (at least in aqueous systems) than had previously been anticipated. Electrostatic forces modify the diffusive lateral migration of small particles ($a < 1\ \mu$m) if the solvent has a low ionic strength. Unusual separation behavior is observed when the capillary radius is small or the solvent flowrate is very low, as evidenced by the non-monotonic calibration curves. These results highlight the delicate balance between diffusion and inertial force, especially in the transition regime, and the underlying complexity of particle–capillary hydrodynamics and electrostatics.

An important conclusion is that the separation of particle mixtures in narrow size ranges can be achieved through careful choice of experimental conditions. Flat sections of calibration curves produce large differences in retention ratio for particles of only slightly different size. Such flat sections coincide with the transition from inertia- to diffusion-controlled lateral migration. Proper choice of ionic strength can result in a broad transition region leading to strong separation of particles in a narrow size range. The particular size range can be chosen through variation of the solvent flowrate. Careful selection of the capillary radius in conjunction with other system parameters prevents non-monotonic separation behavior.

Poor quantitative agreement between the theoretical and experimental retention ratios for large particles is a consequence of an inaccurate model of inertial lateral migration for the conditions considered. We have essentially extrapolated the analysis of Ishii & Hasimoto (1980) from asymptotically small particles at infinite dilution to the regime of finite particle Reynolds numbers and concentrations. The error in the calculation is most apparent in the predicted values of r^* which determine the elution speed of large, inertially dominated particles. Ishii & Hasimoto's value of $r^* = 0.71$ implies that large particles pass through the capillary *more slowly* than an average unit of solvent, a result at odds with most tubular pinch data. Walz & Grun's (1973) empirical correlation of published r^* data is introduced so that particles are eluted faster than the solvent, in qualitative agreement with experiment. An additional empirical parameter produces a fit of Noel *et al.*'s (1982) experimental calibration curve, but the matching may not be unique and is not as yet supported by any theoretical arguments. The point is that a better quantitative prediction of large particle separation by CHDC requires an analysis of inertial lateral migration valid at larger particle Reynolds numbers and possibly at finite concentrations.

Further CHDC experiments are warranted, as well. Measurement of the retention ratios of large particles of known size can be used to determine the equilibrium radial position of the translating particles. This idea, briefly discussed by Noel *et al.* (1982), is an improvement over previous tubular pinch experiments (Segré & Silberberg 1962a, b; Jeffrey & Peterson 1965; Tachibana 1973) which relied upon optical measurement of particle positions. Other techniques, such as flow-field fractionation (FFF), provide a comparable means of analyzing the inertial force as well as other colloidal forces. For example, Caldwell *et al.* (1979) observe flowrate-dependent retention ratios in their sedimentation FFF experiments. They speculate that such behavior is due to a lift (i.e. inertial) force in the particle-plane flow system. A more complete theoretical analysis of FFF, performed by Prieve (1983), considers axial dispersion in both the long retention time limit (equivalent to the Brenner–Gaydos analysis) and the short retention time (non-Brownian) limit. Prieve's analysis in the latter limit may be more relevant to CHDC experiments than the approach used here, at least for the characterization of submicron sized particles. For larger particles, the retention ratio depends critically on the location of the equilibrium radial position, and so precise characterization of the functional dependence of r^* upon particle size and solvent flowrate is a requirement for complete, quantitative understanding of inertial effects in CHDC.

REFERENCES

ARIS, R. 1956 On the dispersion of a solute in a fluid flowing through a tube. *Proc. R. Soc. Lond.* **A235,** 67–77.

BELL, G. M., LEVINE, S. & MCCARTNEY, L. N. 1970 Approximate methods of determining the double-layer free energy of interaction between two charged colloidal spheres. *J. Colloid Interface Sci.* **33,** 335–359.

BRENNER, H. 1966 Hydrodynamic resistance of particles at small Reynolds numbers. *Adv. chem. Engng* **6,** 287–438.

BRENNER, H. 1972 Dynamics of neutrally buoyant particles in low Reynolds number flows. *Prog. Heat Mass Transfer* **6,** 509–574.

BRENNER, H. & GAYDOS, L. J. 1977 The constrained Brownian movement of spherical particles in cylindrical pores of comparable radius. *J. Colloid Interface Sci.* **58,** 312–356.

BRENNER, H. & HAPPEL, J. 1958 Slow viscous flow past a sphere in a cylindrical tube. *J. Fluid Mech.* **4,** 195–213.

BRETHERTON, F. P. 1962 The motion of rigid particles in a shear flow at low Reynolds numbers. *J. Fluid Mech.* **14,** 284.

BROUGH, A. W. J., HILLMAN, D. E. & PERRY, R. W. 1981 Capillary hydrodynamic chromatography—an investigation into operational characteristics. *J. Chromat.* **208,** 175–182.

CALDWELL, K. D., NGUYEN, T. T., MYERS, M. N. & GIDDINGS, J. C. 1979 Observations on anomalous retention in steric flow-field fractionation. *Sepn Sci. Technol.* **14,** 935–946.

COX, R. G. & BRENNER, H. 1968 The lateral migration of solid particles in Poiseuille flow. I. Theory. *Chem. Engng Sci.* **23,** 147–173.

COX, R. G. & HSU, S. K. 1977 The lateral migration of solid particles in a laminar flow near a plane. *Int. J. Multiphase Flow* **3,** 201–222.

DIMARZIO, E. A. & GUTTMAN, C. M. 1969 Separation by flow. *Polym. Lett.* **7,** 267–272.

DIMARZIO, E. A. & GUTTMAN, C. M. 1970 Separation by flow. *Macromolecules* **3,** 131–146.

GOLDMAN, A. J., COX, R. G. & BRENNER, H. 1967 Slow viscous motion of a sphere parallel to a plane wall. II. Couette flow. *Chem. Engng Sci.* **22,** 653.

HAPPEL, J. & BRENNER, H. 1983 *Low Reynolds Number Hydrodynamics*, 2nd edn. Martinus Nijhoff, Dordrecht, The Netherlands.

HIRSCHFELD, B. R., BRENNER, H. & FALADE, A. 1984 First- and second-order wall effects upon slow viscous assymmetric motion of an arbitrarily-shaped, -positioned, and -oriented particle within a circular cylinder. *Physicochem. Hydrodynam.* **5,** 99–133.

ISHII, K. & HASIMOTO, H. 1980 Lateral migration of a spherical particle in flows in a circular tube. *J. phys. Soc. Japan* **48,** 2144–2155.

JEFFREY, R. C. & PEARSON, J. R. A. 1965 Particle motion in laminar vertical tube flow. *J. Fluid Mech.* **22,** 721–735.

LEAL, L. G. 1980 Particle motions in a viscous fluid. *A. Rev. Fluid Mech.* **12,** 435–476.

MCHUGH, A. J. 1984 Particle size measurement using chromatography. *CRC crit. Rev. analyt. Chem.* **15,** 63–117.

MULLINS, M. E. & ORR, C. 1978 Particle sizing by capillary hydrodynamic chromatography. *Int. J. Multiphase Flow* **5,** 79–85.

NAGY, D. J., SILEBI, C. A. & MCHUGH, A. J. 1981 Hydrodynamic chromatography—an evaluation of several features. *J. Colloid Interface Sci.* **79,** 264–267.

NOEL, R. J., GOODING, K. M., REGNIER, F. E., BALL, D. M., ORR, C. & MULLINS, M. E. 1982 Capillary hydrodynamic chromatography. *J. Chromat.* **166,** 373–382.

OSHIMA, H., HEALY, T. W. & WHITE, L. R. 1982 Accurate analytic expressions for the surface charge density/surface potential relationship and double-layer potential distribution for a spherical colloid particle. *J. Colloid Interface Sci.* **90,** 17–26.

PRIEVE, D. C. 1983 Axial dispersion of sedimented colloids. *Sepn Sci. Technol.* **17,** 1587–1607.

PRIEVE, D. C. & HOYSAN, P. M. 1978 Role of colloidal forces in hydrodynamic chromatography. *J. Colloid Interface Sci.* **64,** 201–213.

SAFFMAN, P. G. 1956 On the motion of small spheroidal particles in a viscous liquid. *J. Fluid Mech.* **1,** 540.

SEGRÉ, G. & SILBERBERG, A. 1962a Behavior of macroscopic rigid spheres in Poiseuille flow. Part I. *J. Fluid Mech.* **14,** 115–135.

SEGRÉ, G. & SILBERBERG, A. 1962b Behavior of macroscopic rigid spheres in Poiseuille flow. Part II. *J. Fluid Mech.* **14,** 136–157.

SILEBI, C. A. & MCHUGH, A. J. 1978 An analysis of flow separation in hydrodynamic chromatography of polymer latexes. *AIChE Jl* **24,** 204–212.

SMALL, H. 1974 Hydrodynamic chromatography. *J. Colloid Interface Sci.* **48,** 147–161.

STOISITS, R. F., POEHLEIN, G. W. & VANDERHOFF, J. W. 1976 Mathematical modelling of hydrodynamic chromatography. *J. Colloid Interface Sci.* **57,** 337–344.

TACHIBANA, M. 1973 On the behaviour of a sphere in the laminar tube flows. *Rheol. Acta* **12,** 58–69.

TAYLOR, G. I. 1953 Dispersion of soluble matter in a solvent flowing slowly through a tube. *Proc. R. Soc. Lond.* **A219,** 186–203.

TAYLOR, G. I. 1954 Conditions under which dispersion of a solute in a stream of solvent can be used to measure molecular diffusion. *Proc. R. Soc. Lond.* **A225,** 473–479.

TIJSSEN, R., BLEUMER, J. P. A. & VAN KREVELD, M. E. 1983 Separation by flow (hydrodynamic chromatography) of macromolecules performed in open microcapillary tubes. *J. Chromat.* **260,** 297–304.

WALZ, D. & GRUN, F. 1973 The radial velocity of spherical particles in tubular pinch effect experiments. *J. Colloid Interface Sci.* **45,** 467–477.